공학석사 학위논문

Impingement of a Round Jet on a Circular Pin-Fin Inside the Potential Core

포텐셜 코어 안에서의 원기둥과 원형제트의 충돌

2015 년 8 월

서울대학교 대학원

기계항공공학부

Dylan Barratt

Impingement of a Round Jet on a Circular Pin-Fin Inside the Potential Core

지도 교수 송성진

이 논문을 공학석사 학위논문으로 제출함

2015 년 4 월

서울대학교 대학원

기계항공공학부

Dylan Barratt

딜런배럿의 석사 학위논문을 인준함

2015 년 6 월

위원장 김호영 (인)

부위원장 송성진 (인)

위원 박형민 (인)

Abstract

Impingement of a Round Jet on a Circular Pin-Fin Inside the Potential Core

Dylan Barratt

Department of Mechanical and Aerospace Engineering

Seoul National University

The internal cooling configurations of a turbine blade frequently incorporate pin-fins in the trailing edge. Some blades also incorporate perforated baffles, or "blockages", upstream of the pin-fins. The blockages are intended to augment turbulence. However, an unintended consequence is the exposure of the trailing edge pin-fins to the impingement of round jets. The present study examines the impingement of a round jet on a circular pin-fin / cylinder and aerodynamically explains the heat transfer distribution in the crossflow plane. After stagnation, a second peak in heat transfer has been newly found to be caused by transition of the boundary layer incited by merger of the turbulent mixing layer of the jet with the laminar boundary layer developing on the cylinder surface. Merger results in the termination of the potential core, forming a viscous jet that transports momentum away from the wall causing a monotonic decline in heat

transfer and promoting separation of the boundary layer. However, turbulence and streamline curvature delay separation to the far aft of the cylinder where heat transfer eventually plateaus.

Keywords: turbine blade cooling; blockages; round-jet impingement; pin-fin/cylinder

Student Number: 2013-23824

CONTENTS

1. Introduction……1

2. Experimental Details……..6

3. Free Jet Characteristics……...9

4. Separation Hypothesis……..11

5. Transition Hypothesis……...14

6. Mechanism of Transition……..18

7. Location of Separation……..22

8. Conclusions……..25

9. Acknowledgements……..26

10. References……27

11. Appendix A……..32

LIST OF FIGURES

Figure 1. Turbine blade cooling……...1

Figure 2. The Nusselt number distribution in the crossflow plane at Re_D = 50,000……3

Figure 3. Possible causes of the second peak in heat transfer……..4

Figure 4. Wind-tunnel…….…….7

Figure 5. Test bench…….7

Figure 6. Flow visualisation of the free jet……..9

Figure 7. Velocity distribution along the jet centreline……..10

Figure 8. Shear-stress distribution in the crossflow plane……..12

Figure 9. Calibration of the hot-wire……..15

Figure 10. Calibration curves for the hot-wire probe from before and after an experiment…….....16

Figure 11. Maximum turbulence strength within the boundary layer at various azimuth angles……...17

Figure 12. Flow visualisation of jet impingement……...…….20

Figure 13. Turbulence strength profiles……...21

Figure 14. Time-averaged velocity profiles on the aft of the cylinder…..22

Figure 15. Schematic of the flow-field and heat transfer distribution in the crossflow plane…….…..25

Figure 16. Static pressure distribution in the crossflow plane of a cylinder subject to the impingement of a round jet and immersed in a uniform stream at Re_D = 50,000……..32

LIST OF TABLES

Table 1. Configuration parameters…….8

NOMENCLATURE

A	Proportionality constant of King's law
B	Offset constant of King's law
C_f	Skin friction coefficient
D	Cylinder diameter
D_j	Jet diameter
E	Hot-film sensor voltage
h	Convection coefficient
k_f	Thermal conductivity of air
$\dot{m}$	Mass flowrate
Nu	Nusselt Number
r	Radial jet coordinate
r'	Radial cylinder coordinate
Re_D	Reynolds number
u	Local velocity
u'	Temporal velocity fluctuation
u_{rms}	Root mean square velocity fluctuation
w_e	Centreline velocity at jet nozzle exit
y	Traverse distance
z	Axial jet coordinate
z'	Axial cylinder coordinate

Greek

α	Azimuth angle
δ	Boundary layer thickness
μ	Dynamic viscosity of air
ρ	Density of air
τ_w	Wall-shear
ν	Kinematic viscosity of air

INTRODUCTION

Demand for increased cycle efficiency has caused turbine inlet temperatures to rise beyond the metallurgical limits of the turbine blade material. Blade cooling is therefore necessary and can be accomplished by two means. Film cooling outside the blade inhibits heat transfer to the material and internal cooling inside the blade removes heat from the material. However, the trailing edge of the blade poses particular difficulties. Film cooling near the trailing edge is inhibited by separation of the suction-side boundary layer, and internal cooling is restricted by the aerodynamic requirement for a thin trailing edge which limits the space available for cooling.

The ineffectiveness of both film and internal cooling at the trailing edge necessitates heat transfer enhancement by alternate means such as pin-fins [1-4] (Fig. 1a). Integral casting of the turbine blade with the "lost wax" process [5] allows for complex internal cooling passages, and several blade designs have sought to further enhance heat transfer with perforated baffles upstream of

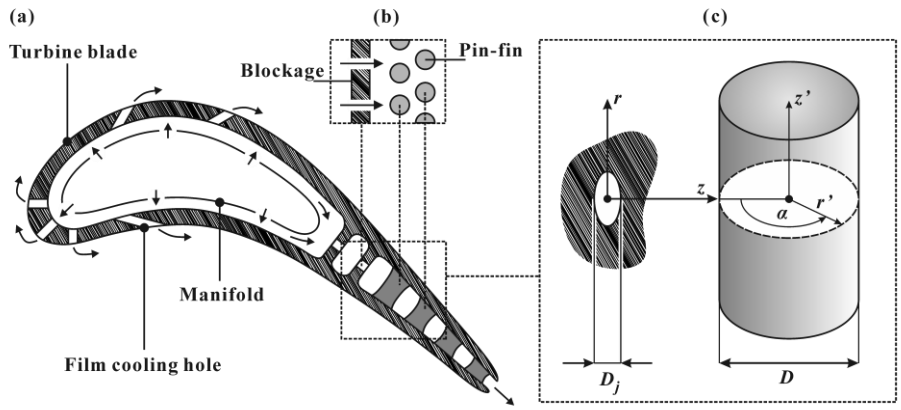

Figure 1. Turbine blade cooling: (a) Film cooling and internal cooling schemes; (b) Trailing edge pin-fins subject to jet impingement; (c) Round jet impingement on a circular pin-fin / cylinder.

the pin-fins, termed “blockages” [6-8]. The blockages are intended to promote turbulence and enhance heat transfer inside the cooling passages [9-13]. However, flow passing through the perforated blockages will form round jets that impinge upon the pin-fins positioned downstream (Fig. 1b). Simplistically, this configuration represents the impingement of a round jet on a circular cylinder (Fig. 1c). The heat transfer attributes of this configuration have been well-documented in literature because of relevance to numerous engineering applications including furnace cooling [14] and the cooling of extruded materials [15]. However, the heat transfer characteristics have not been fully explained.

Previous heat transfer studies have focused on the effects of Reynolds number (Re_D), impingement distance (z/D_j), and diameter ratio (D/D_j) on overall heat transfer [16], stagnation point heat transfer [14, 17-19], and the circumferential and axial distributions of heat transfer for both constant temperature [17] and constant heat flux [14, 18-21] conditions. The heat transfer distribution in the “crossflow” (r', α) plane, which coincides with the jet axis, is depicted in Fig. 2 with the Nusselt number ($Nu=hD/k_f$) portrayed on the ordinate and azimuth angle (α) on the abscissa. The Nusselt number comprises of the convection coefficient (h) the thermal conductivity of air (k_f) and the cylinder diameter (D). The highest heat transfer occurs at the stagnation point ($\alpha = 0°$) and declines away from the stagnation point ($0° < \alpha < 40°$) due to increasing boundary layer thickness [16, 17]. However, the decline is sometimes interrupted by a second peak in heat transfer ($40° < \alpha < 80°$) which contributes significantly to the overall heat transfer [14]. Yet, the mechanism of the second peak has not been conclusively determined.

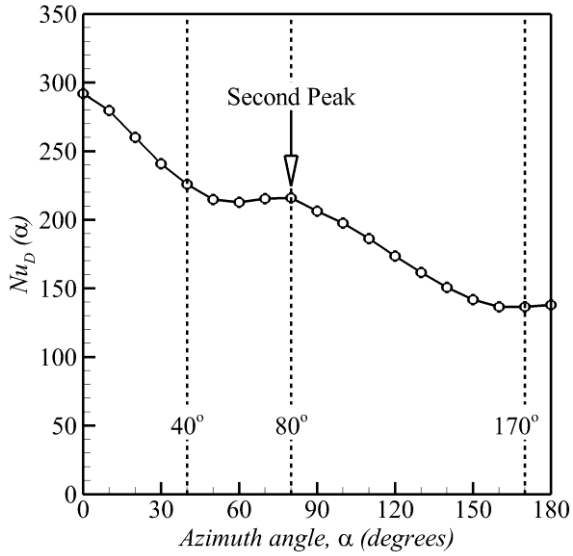

Figure 2. The Nusselt number distribution in the crossflow plane at Re_D = 50,000 [14].

The local minimum in heat transfer that precedes the second peak is a commonly accepted indicator of boundary layer separation [22], suggesting that the second peak may be caused by enhanced heat transfer in the recirculation zone (Fig. 3a). Support for the separation argument has been provided by two-dimensional "slot" jet investigations by Hsueh & Chin [23], Bartoli et al. [24] and a round jet study performed by Fleischer et al. [25]. All these studies considered jet impingement on a cylindrical surface and reported separation on the fore of the cylinder ($35° < \alpha < 60°$) in the vicinity of the second peak.

On the contrary, slot jet experiments performed by Schuh & Persson [26], Kumada et al. [27], Sparrow & Alhomoud [28] and round jet numerical simulations performed by Singh et al. [18, 19] reported separation on the far aft

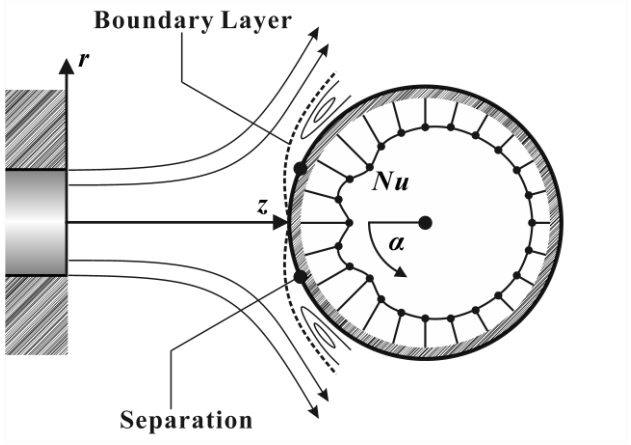

(a)

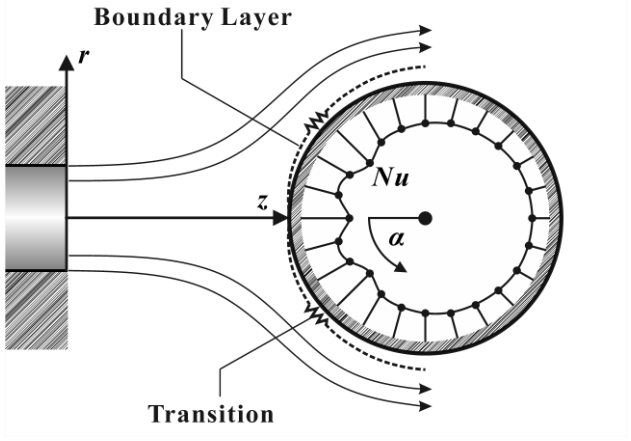

(b)

Figure 3. Possible causes of the second peak in heat transfer: (a) separation; (b) transition.

of the cylinder. Separation of the boundary layer is characteristically associated with an inflection in the static pressure distribution for a cylinder in crossflow [29]; the absence of an inflection (Appendix A) led Wang et al. [14] to argue that the second peak could not be a result of separation but rather a result of boundary layer transition (Fig. 3b). The boundary layer that develops after

stagnation must initially be laminar and transition is known to enhance local heat transfer which could cause the second peak. However, the association between separation and an inflection in static pressure derives from a cylinder in a free-stream and may not necessarily hold for jet impingement.

It still remains unclear whether separation or transition is responsible for the second peak in heat transfer and the heat transfer distribution in the crossflow plane remains unexplained. Therefore, the objectives of the present study are to: (1) investigate the flowfield and determine if/where separation and transition of the boundary layer occur and, thus, (2) explain the heat transfer distribution in the crossflow plane, including the cause for the second peak in heat transfer.

EXPERIMENTAL DETAILS

The pin-fin configuration used by Krause et al. [6] employs a diameter ratio (D/D_j) of 2 with impingement distances (z/D_j) between 2 and 4. The short impingement distance is a typical result of the confined space within the blade. The Reynolds (Re_D) number, defined in Eq. (1), encountered by pin-fins inside of a turbine blade ranges between 5,000 and 50,000 [4].

$$\mathrm{Re}_D = \frac{w_e D}{\nu} \tag{1}$$

The characteristic length is the diameter of the cylinder (D) and the characteristic velocity is the centreline velocity at the jet exit (w_e). The kinematic viscosity of air is denoted by ν. Wang et al. [14] tested a configuration similar to that of Krause et al. [6] and observed a second peak in heat transfer in the crossflow plane. The present study has used the same configuration as Wang et al. [14] (Table 1).

Testing has been performed with a facility at Seoul National University, Seoul, Korea. The air supply consists of a small-scale wind tunnel (Fig. 4) featuring a 22 kW centrifugal blower which passes flow through a volute into a plenum chamber containing honeycomb and mesh flow straighteners. Flow from the plenum chamber passes through a sudden contraction intended to

Table 1. Configuration parameters.

	D/D_j	z/D_j	Re_D
Turbine blade [6]	2	2 – 4	5,000 – 50,000
Present study / Wang et al. [14]	2.5	2	50,000

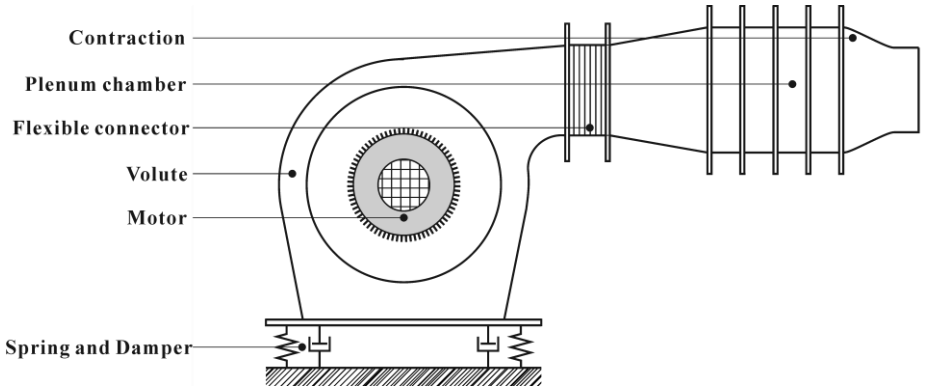

Figure 4. Wind tunnel.

improve flow uniformity at the nozzle exit with a freestream turbulence intensity of approximately 0.5% and a maximum volumetric flowrate of approximately 80 m^3/min which corresponds to a Reynolds number of 700,000 based on the nozzle diameter. Vibration has been minimised by mounting the blower on spring-and-damper supports while flexible tubing has been used to connect the blower and plenum chamber of the wind tunnel in a further effort to isolate the test bench from vibration. The air supply from the wind tunnel passes to the test bench (Fig. 5) which includes another plenum chamber with further flow straighteners followed by a sudden contraction that terminates with the jet nozzle. The target cylinder has been mounted on a rotary table (Velmex B4800TS) to allow for angular rotation while a linear traverse system (Velmex BiSlide®) has been used to perform measurements in the radial direction.

Several simplifying assumptions distinguish the test configuration from the actual application. Firstly, pin-fins in application are of low aspect ratio (Fig. 1a) resulting in significant end-wall effects; however, such effects have not

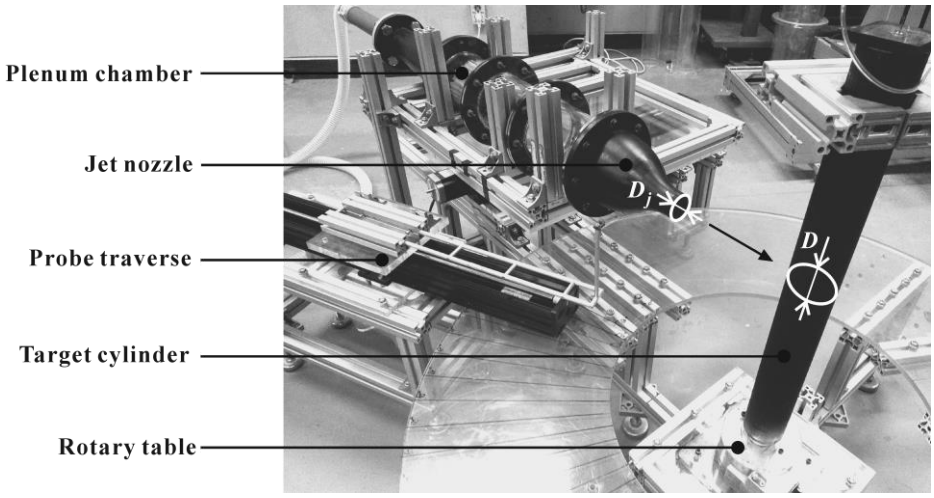

Figure 5. Test bench.

been considered by the present study. Secondly, offset between the axis of the jet and the axis of the pin-fin / cylinder (Fig. 1b) may arise in application but has not been considered here. Thirdly, closely spaced pin-fins may experience a proximity effect due to flow acceleration between the pin-fins; however, the present study only considers a single cylinder in isolation. Fourthly, inside a turbine blade, the blockage holes may be angled toward the blade suction surface for additional impingement cooling which results in axial inclination of the jets relative to the pin fins. However, the present study only considers normal impingement of the jets. Lastly, cooling flow within a rotating blade would also experience the Coriolis effect and centrifugal forces that may influence the jet characteristics [30], but they have not been considered in this study. The present study is, thus, restricted to the simplest case of a round jet impinging on a long circular cylinder without offset, inclination, or proximity effects, in the absence of rotation.

FREE JET CHARACTERISTICS

Characterisation of the jet has been performed with flow visualisation. The jet has been seeded with vegetable oil and illuminated with a Nd:YAG laser along the centreline with image capturing by a charge-coupled-device (CCD) camera (Fig. 6). Immediately after leaving the nozzle, a mixing layer develops at the edge of the jet as instability of the laminar shear layer causes roll-up into periodic, coherent vortex structures in the transitional region ($z/D_j < 3.0$) [31]. Growth of wave instabilities and entanglement degrades the vortices into incoherent turbulent eddies of varying scales in the turbulent region ($z/D_j > 3.0$) [31]. The centre of the jet is initially undisturbed by the presence of the mixing layer at the jet periphery. Eventually, the mixing layer penetrates to the centre of the jet, terminating the potential core, and merging to form a fully developed jet. The distance from the nozzle exit to the location of mixing layer merger is referred to as the "potential core" length, usually found to be $4.7 < z/D_j < 7.7$ [32].

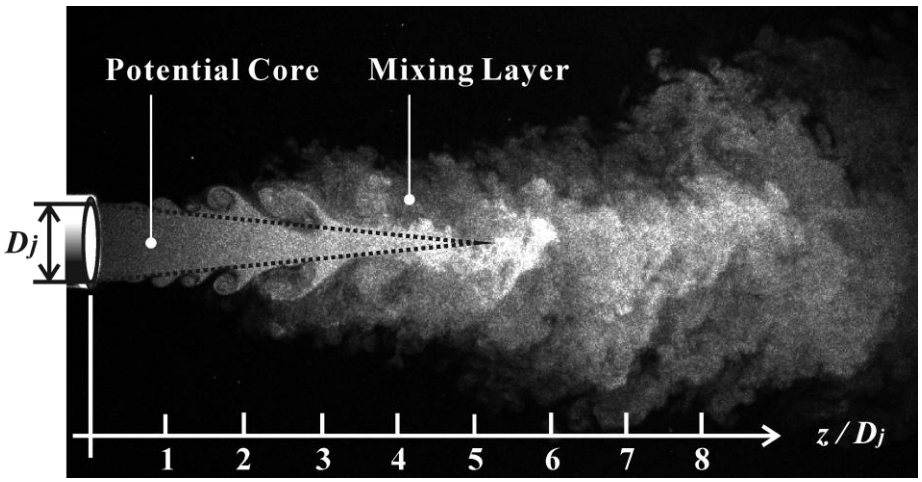

Figure 6. Flow visualisation of the free jet.

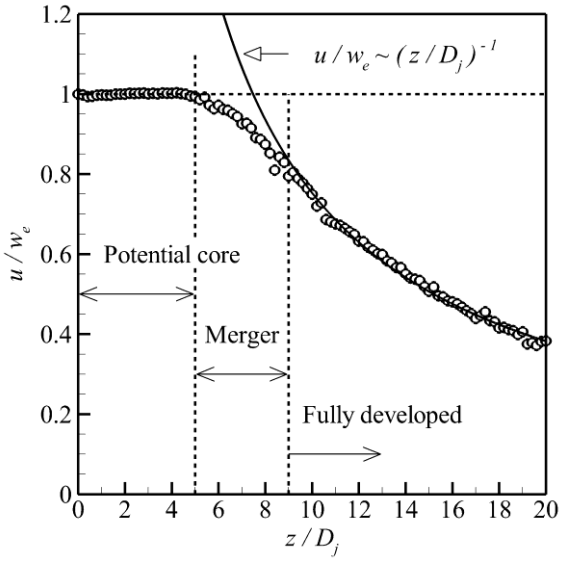

Figure 7. Velocity distribution along the jet centreline.

The potential core length in this study may be visually estimated from Fig. 6 and found to be approximately 5.0 D_j. To quantitatively confirm the length of the potential core in this study, the velocity along the centreline of the jet ($r = 0$) has been measured with a Pitot probe (Fig. 7). The velocity (u / w_e) at the centre of the jet remains constant until $z/D_j = 5.0$, consistent with the qualitative estimate of Fig. 6. Thereafter, the mixing layers merge ($5.0 < z/D_j < 9.0$) and a fully developed jet is formed ($z/D_j = 9.0$) where the centreline velocity becomes inversely proportional to z/D_j [33].

SEPARATION HYPOTHESIS

Separation of the boundary layer is characteristically associated with zero wall-shear on the cylinder surface. Therefore, the shear stress distribution in the crossflow plane has been measured to determine whether separation is the cause for the second peak in heat transfer. The shear-stress distribution has been measured with a single hot-film sensor (55R47 Dantec Inc.) of thickness 50 μm which has been flush mounted on the cylinder surface. The cylinder has been rotated with a rotary table for $0° \leq \alpha \leq 180°$ at 5° intervals with an uncertainty of ±0.2°.

Calibration has been performed by immersing the cylinder and mounted sensor in a free-stream. The voltage of the sensor (E) has been recorded at a specific azimuth angle and calibrated against the wall-shear (τ_w) calculated from a velocity profile measured at the same azimuthal location using hot-wire anemometry, in accordance with the method of Desgeorges et al. [34]. This procedure has been repeated for a range of free-stream velocities allowing voltage (E) and wall-shear (τ_w) to be correlated with King's law [35, 36]:

$$\tau_w^{1/3} = AE^2 + B \tag{2}$$

where A and B are the empirical constants determined from linear regression of the data, and τ_w is the wall-shear defined as:

$$\tau_w = \mu \left. \frac{du}{dy} \right|_{y=0} \tag{3}$$

Here, u is the velocity component parallel to the wall, y is the direction normal to the wall, and μ denotes the dynamic viscosity of air. The shear stress has been normalised to determine the skin friction coefficient (C_f):

$$C_f = \frac{\tau_w}{\frac{1}{2}\rho w_e^{\,2}} \tag{4}$$

The wall shear stress measurement is shown in Fig. 8 with the skin friction coefficient (C_f) on the ordinate plotted against azimuth angle (α) on the abscissa. The experimental uncertainty in C_f has been estimated at 4.4% using a method reported in Holman [37]. Zero skin friction occurs at the leading edge of the cylinder (α = 0°) due to stagnation. Thereafter, the wall shear rises sharply due to flow acceleration away from the stagnation point. The rise in shear is, however, counteracted by a competing effect – the diffusion of momentum

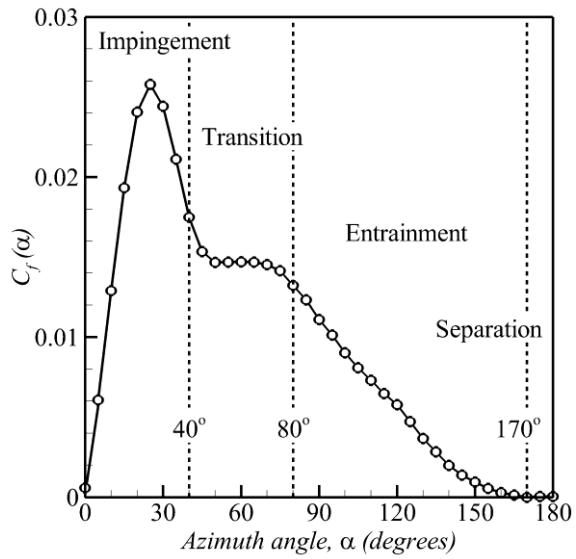

Figure 8. Shear-stress distribution in the crossflow plane.

away from the wall caused by thickening of the boundary layer. Shear therefore peaks at 25° and thereafter begins to decline. The decline is, however, interrupted by a plateau in shear that occurs in the known vicinity of the second peak in heat transfer. This plateau in C_f at a non-zero value excludes separation as a cause for the second peak.

TRANSITION HYPOTHESIS

Elimination of separation leaves transition as the remaining possible mechanism for the second peak in heat transfer. The plateau in shear (Fig. 8) may also be explained by transition since boundary layer growth is known to reduce wall-shear while transition is known to increase wall-shear. To confirm transition of the boundary layer, time-resolved velocity measurements have been performed at different azimuthal locations (α) on the cylinder surface to calculate turbulence properties inside the boundary layer.

The time-resolved velocity measurements have been performed with hot-wire anemometry using a straight single-sensor probe (Dantec Dynamics 55P11) at a sampling frequency of 10 kHz for a duration of 10 seconds at each measurement point. The probe has been traversed normal to the cylinder surface at azimuthal locations (α) between 30° and 150° in 10° intervals. Measurements at azimuth angles (α) less than 30° and greater than 150° have not been taken because flow cannot be assumed parallel to the cylinder surface and a single-sensor probe cannot indicate flow direction.

The hot-wire probe (Figure 9a) has been calibrated immediately before each experiment by placing the probe inside a wind-tunnel alongside a Pitot probe in combination with a differential pressure transducer (NetScanner 9116), with air supply from the described wind-tunnel. The hot-wire probe and Pitot probe have been adjacently mounted at the exit of the wind-tunnel nozzle (Figure 9b). Flow velocity at the nozzle exit has been adjusted with a frequency controller to cover the range of velocities encounter by the hot-wire probe during measurements.

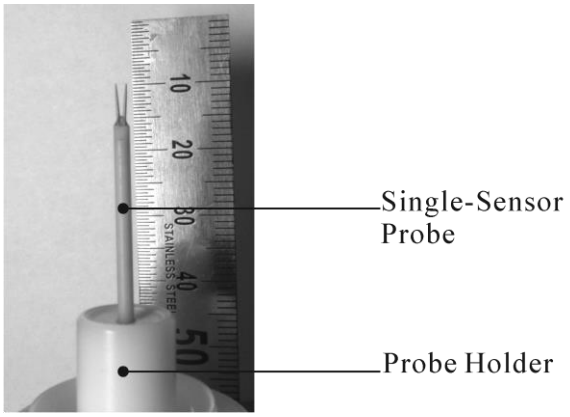

(a)

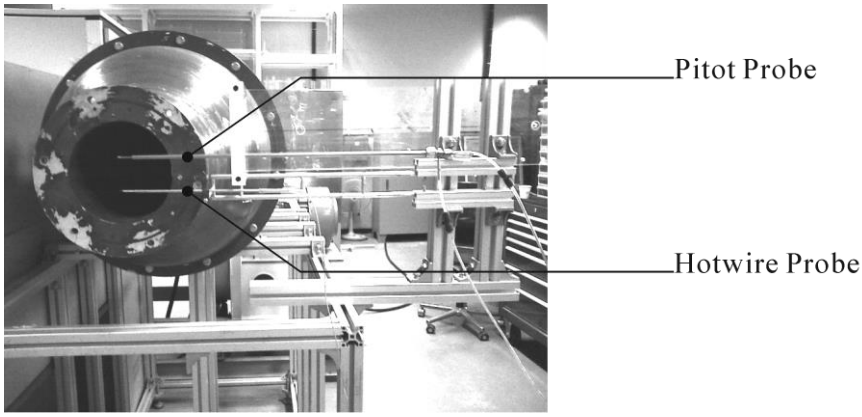

(b)

Figure 9. Calibration of the hot-wire; (a) Dantec dynamics 55P11 straight single-sensor hot-wire probe; (b) calibration configuration.

A critical concern of hot-wire anemometry is the error introduced by change in ambient temperature during a measurement [38]. Ambient temperature has been recorded at the start and end of each experiment with a maximum discrepancy of 1.8 Kelvin. The extent of ambient temperature effects has been investigated by calibrating the probe immediately before and after experiments, with a typical comparison depicted in Fig. 10. A maximum deviation of 0.6% occurs between the two calibration curves.

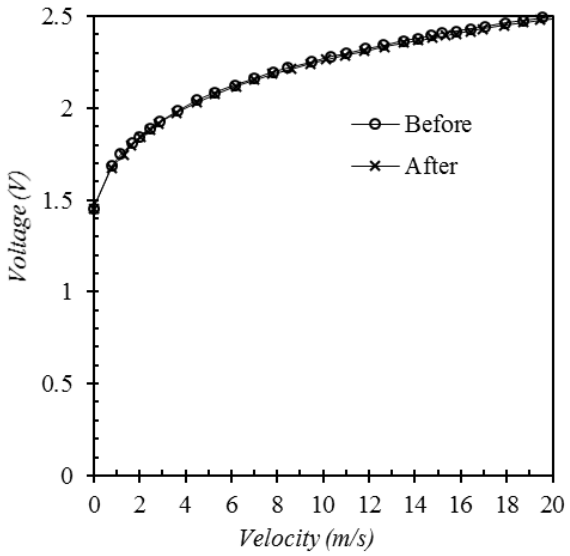

Figure 10. Calibration curves for the hot-wire probe from before and after an experiment.

The time-resolved velocity measurements have been used to calculate the turbulence strength (u_{rms}), defined as:

$$u_{rms} = \sqrt{\frac{1}{N}\sum_{1}^{N}\left(u_i^{'}\right)^2} \tag{5}$$

where u'_i denotes the measured instantaneous velocity fluctuation and N represents the number of data points. In this study, the boundary layer has been defined as the region between the wall and the point of peak velocity. The maximum turbulence strength within the boundary layer (u_{rms}) has been normalised by the centreline velocity at the jet exit (w_e) and plotted against azimuth angle (α) in Fig. 11. The maximum experimental uncertainty of

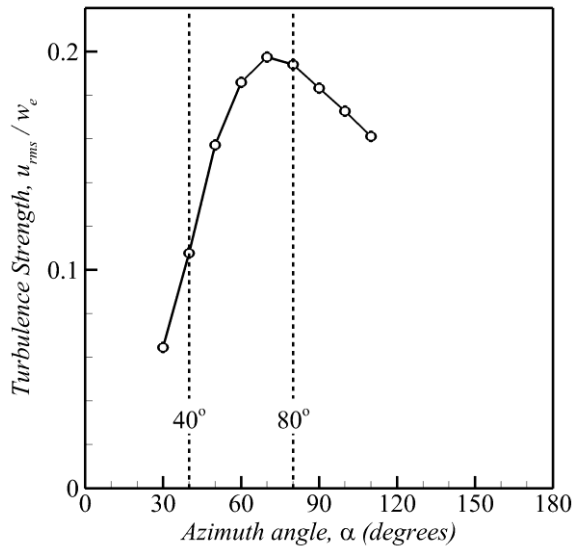

Figure 11. Maximum turbulence strength (u_{rms} / w_e) within the boundary layer.

u_{rms} / w_e values in Fig. 11 has been estimated at 0.8% using a method reported in Holman [37]. A dramatic rise in turbulence strength inside the boundary layer can be seen between 40° and 80°. Thus, the plateau in shear and the second peak in heat transfer are due to transition of the boundary layer.

MECHANISM OF TRANSITION

The present study also seeks to explain how the boundary layer transitions. The turbulent mixing layer formed at the edge of the jet consists of coherent structures which degrade into turbulent eddies of varying scales (Fig. 12a) [31]. Two previous slot jet studies [26, 27] suggest that growth of the mixing layer transports turbulence inwards from the jet periphery promoting transition of the boundary layer on the cylinder surface. The present study seeks to confirm this assertion with the hypothesis that transition occurs specifically at the point where the turbulent mixing layer merges with the laminar boundary layer on the cylinder surface (Fig. 12b).

Figure 13 depicts the turbulence strength profiles measured at $\alpha = 30°$ and $\alpha = 60°$, respectively. The ordinate (y/D) indicates the normal distance away from the wall and the abscissa indicates the turbulence strength (u_{rms}) normalized by the centreline velocity at the jet exit (w_e). Experimental uncertainty has been indicated with error bars calculated with a method reported in Holman [37]. The thickness of the boundary layer (δ) has been calculated from measured velocity profiles and has been indicated in the figures. Since transition of the boundary layer begins around 40°, the boundary layer is expected to be laminar at $\alpha = 30°$ and the mixing layer is anticipated to be separated from the boundary layer by the potential core. Figure 13a supports this argument indicating low turbulence strength inside the boundary layer ($u_{rms} / w_e \approx 6\%$) and the peak in turbulence strength (which indicates the presence of the mixing layer) away from the boundary layer. Since transition of the boundary layer begins around 40° and ends near 80°, the boundary layer is expected to be transitional at $\alpha = 60°$ and the mixing layer is anticipated to have

merged with the boundary layer leading to the disappearance of the potential core. Figure 13b shows that the boundary layer at $\alpha = 60°$ exhibits substantially higher turbulence strength (u_{rms} / $w_e \approx 18\%$) and the peak in turbulence associated with the mixing layer exists adjacent to the boundary layer with no evidence of a potential core in between. Figure 13, thus, confirms that the turbulent mixing layer merges with the laminar boundary layer on the cylinder surface leading to the disappearance of the potential core and transition of the boundary layer.

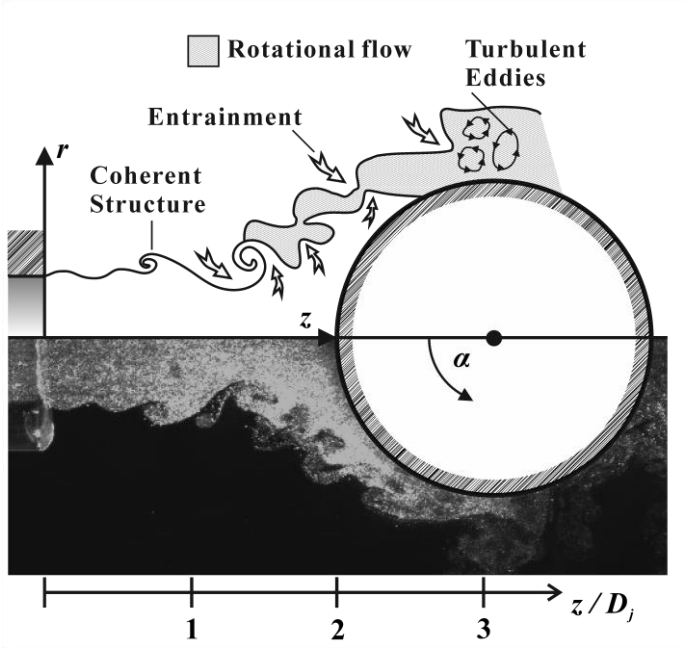

(a)

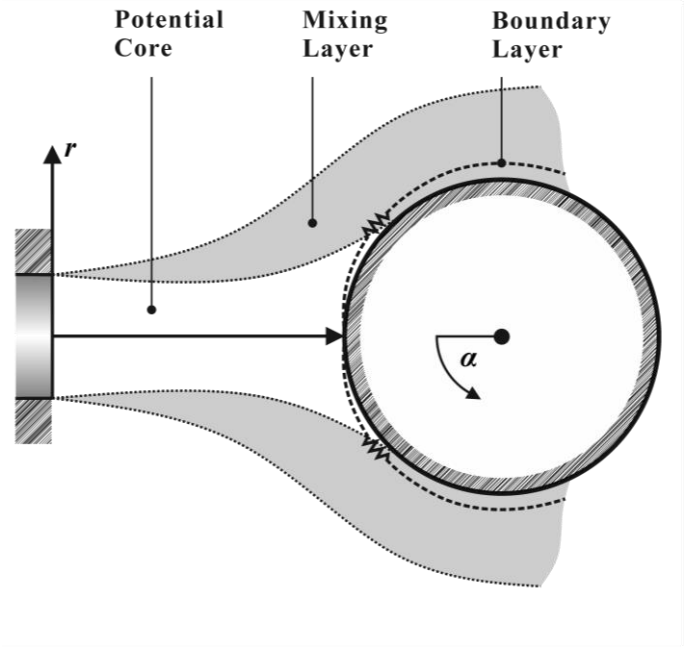

(b)

Figure 12. Flow visualisation of jet impingement: (a) instantaneous flow field; (b) time-averaged flow field.

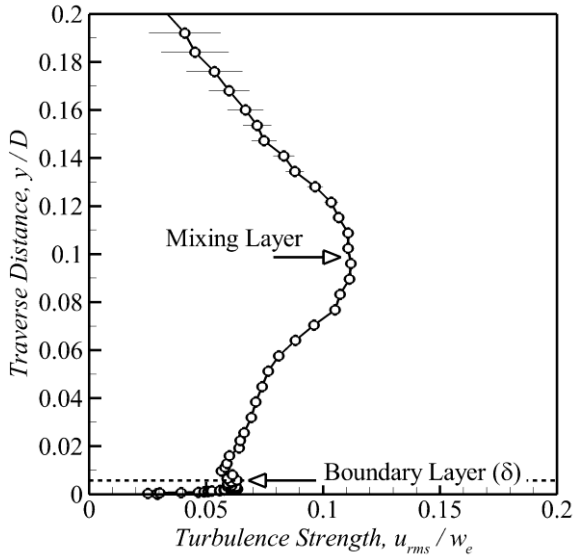

(a)

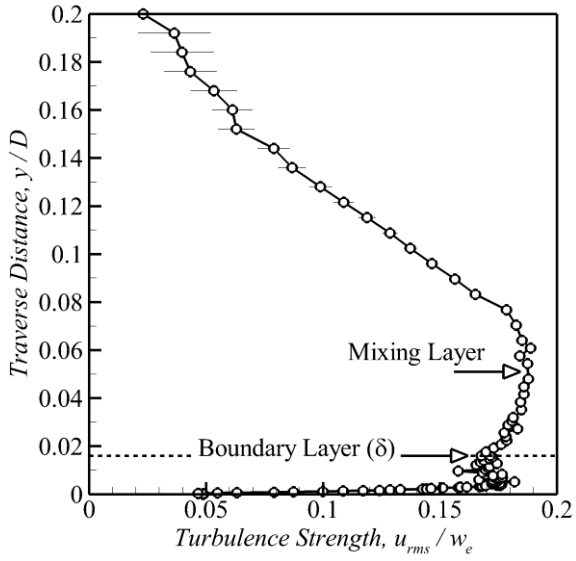

(b)

Figure 13. Turbulence strength profiles (a) before merger, α = 30° and (b) after merger, α = 60°.

LOCATION OF SEPARATION

Following transition, the monotonic decline in shear (Fig. 8) and heat transfer (Fig. 2) on the aft of the cylinder has been investigated with time-averaged velocity profiles, calculated from the hot-wire measurements (Fig. 14). The abscissa of Fig. 14 comprises of the local velocity (u) normalized by the centreline velocity at the jet exit (w_e) and the ordinate comprises of the traverse distance normal to the wall (y) normalized by the diameter of the cylinder (D). Experimental uncertainty has been indicated with error bars calculated according to Holman [37]. Velocity profiles at azimuth angles (α) of 90°, 120° and 150° are shown. Figure 14 reveals that a thickening boundary layer (δ) and diminishing peak jet velocity causes the monotonic decline in shear and heat transfer on the aft of the cylinder. However, growth of the boundary layer in this region is aggravated by the additional effect of entrainment.

After transition, the mixing layer and boundary layer have merged leading

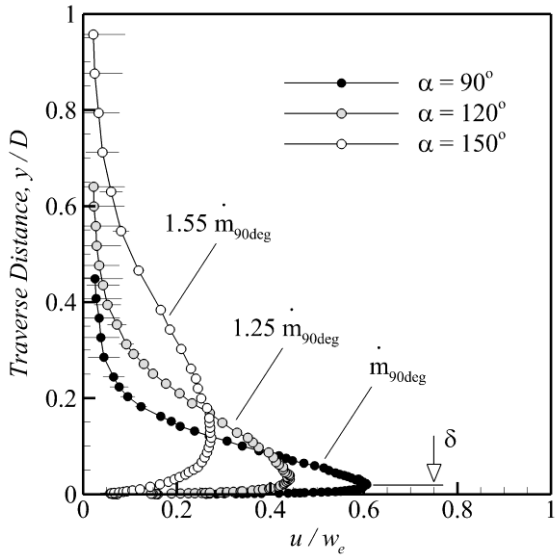

Figure 14. Time-averaged velocity profiles on the aft of the cylinder.

to the disappearance of the potential core and the formation of a viscous jet containing eddies that entrain quiescent surrounding flow into the jet (Fig. 12a) [31], thereby transporting momentum away from the wall. To confirm the occurrence of entrainment, the mass flux of the jet at different azimuth angles (α) has been calculated with numerical integration of the velocity profiles in Fig. 14. A 25% increase in mass flux occurs from 90° to 120° and a 55% increase in mass flux occurs from 90° to 150°, confirming that quiescent surrounding flow has been entrained into the jet thereby aggravating boundary layer growth.

Thickening of the boundary layer increases susceptibility to separation, and previous results have shown that an adverse pressure gradient does exist on the aft of the cylinder (Appendix A). However, the shear stress distribution (Fig. 8) only reaches zero near 170°, where separation occurs (which validates the numerical simulation results of Singh et al. [18, 19]). Such delayed separation suggests the existence of a competing effect that inhibits separation. Previous experiments performed with a slot jet have claimed that delayed separation is a result of the "coanda effect" [26, 27] which has been attributed to a highly turbulent boundary layer [26]. In kinematic terms, the delay in separation may be explained with a streamline curvature argument supported by Lighthill [39] and Wille & Fernholz [40]: a jet passing over a curved surface must exhibit a smaller radius of curvature near the surface than away from the surface. The difference in streamline curvature generates a radial pressure gradient that exerts a centripetal force on the jet thereby suppressing separation of the boundary layer.

In essence, the location of separation for the boundary layer is determined by competing effects. Streamline curvature and turbulence suppress separation

of the boundary layer. However, the gradual transport of momentum away from the wall combined with a weak adverse pressure gradient brings the boundary layer progressively closer to separation which eventually does occur at an azimuth angle (α) near 170°. Thus, the location of separation coincides with the location of zero wall-shear (Fig. 8) and a plateau in the heat transfer distribution (Fig. 2) formed by the weakly circulating wake.

CONCLUSIONS

If the cylinder is positioned within the potential core of the jet (Fig. 15), the heat transfer distribution in the crossflow plane is known to exhibit peak heat transfer at the stagnation point followed by a decline and then a second peak. The present study has concluded that:

- The second peak in heat transfer is caused by transition of the boundary layer, which occurs at the point where the turbulent mixing layer merges with the laminar boundary layer developing on the cylinder surface.
- The merger leads to the disappearance of the potential core forming a viscous jet that aggravates boundary layer growth by entraining the quiescent surrounding flow, which causes a monotonic decline in heat transfer following transition.
- Thickening of the boundary layer promotes separation. However, streamline curvature and turbulence delay separation to the far aft of the cylinder ($\alpha \approx 170°$) where a plateau in heat transfer indicates a weakly circulating wake.

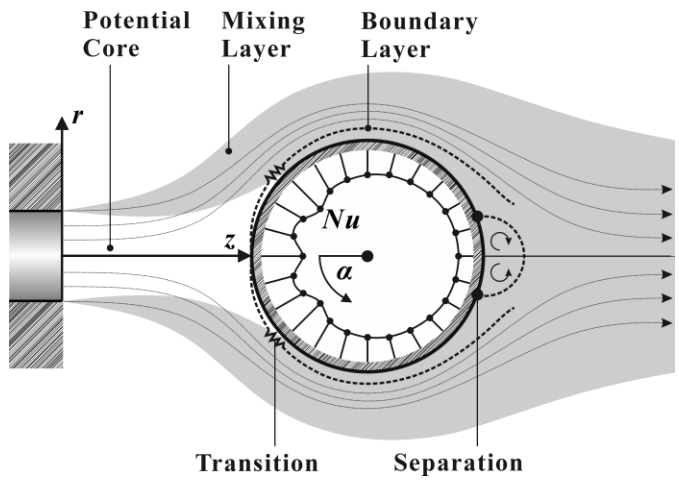

Figure 15. Schematic of the flow-field and heat transfer distribution

REFERENCES

[1] Armstrong, J., and Winstanley, D., 1988, "A Review of Staggered Array Pin Fin Heat Transfer for Turbine Cooling Applications," ASME J. Turbomach., **110**(1), pp. 94-103.

[2] VanFossen, G. J., 1982, "Heat-Transfer Coefficients for Staggered Arrays of Short Pin Fins," ASME J. Eng. Gas Turbines Power, **104**(2), pp. 268-274.

[3] Metzger, D. E., Berry, R. A., and Bronson, J. P., 1982, "Developing Heat Transfer in Rectangular Ducts with Staggered Arrays of Short Pin Fins," ASME J. Heat Transfer, **104**(4), pp. 700-706.

[4] Metzger, D. E., Fan, Z. X., and Shepard, W. B., 1982, "Pressure Loss and Heat Transfer Through Multiple Rows of Short Pin Fins," Heat Transfer 1982, **3**, pp. 137-142.

[5] Power, D. C., 1995, "Palladium Alloy Pinning Wires for Gas Turbine Blade Investment Casting," Platin. Met. Rev., **39**(3), pp. 117-126.

[6] Krause, D., Soechting, F., Mongillo, D., and Zelesky, M., inventors; United Technologies Corporation, assignee, 1999, "Airfoil Cooling," European Patent 0 896 127.

[7] Dally, G. M., McCall, R. A. B., and Evans, P. A., inventors; Rolls-Royce plc, assignee, 2000, "Cooled Aerofoil for a Gas Turbine Engine," European Patent 1 022 432.

[8] Soechting, F., Hada, S., Kuwabara, M., Masada, J., and Tomita, Y., inventors; Mitshubishi Heavy Industries, Ltd., assignee, 2004, "Cooling Structure of Stationary Blade, and Gas Turbine," US Patent 6,761,529.

[9] Lau, S. C., Cervantes, J. C., Han, J. C., and Rudolph, R. J., 2008, "Internal Cooling near the Trailing Edge of a Gas Turbine Airfoil with Cooling Airflow

Through Blockages with Holes," ASME J. Turbomach., **130**(3), p. 031004.

[10] Ahn, H. S., Lee, S. W., Lau, S. C., and Banerjee, D., 2007, "Mass (Heat) Transfer Downstream of Blockages with Round and Elongated Holes in a Rectangular Channel," ASME J. Heat Transfer, **129**(12), pp. 1676-1685.

[11] Moon, S. W., and Lau, S. C., 2003, "Heat Transfer Between Blockages with Holes in a Rectangular Channel," ASME J. Heat Transfer, **125**(4), pp. 587-594.

[12] Chung, H., Park, J. S., Sohn, H. S., Rhee, D. H., and Cho, H. H., 2014, "Trailing Edge Cooling of a Gas Turbine Blade with Perforated Blockages with Inclined Holes," Int. J. Heat Mass Transfer, **73**, pp. 9-20.

[13] Choi, J. H., Mhetras, S., Han, J. C., Lau, S. C., and Rudolph, R., 2008, "Film Cooling and Heat Transfer on Two Cutback Trailing Edge Models with Internal Perforated Blockages," ASME J. Heat Transfer, **130**(1), p. 012201.

[14] Wang, X. L., Motala, D., Lu, T. J., Song, S. J., and Kim, T., 2014, "Heat Transfer of a Circular Impinging Jet on a Circular Cylinder in Crossflow," Int. J. Therm. Sci., **78**, pp. 1-8.

[15] Miyazaki, H., and Sparrow, E. M., 1976, "Potential Flow Solution for Crossflow Impingement of a Slot Jet on a Circular Cylinder," ASME J. Fluids Eng., **98**(2), pp. 249-255.

[16] Sparrow, E. M., Altemani, C. A. C., and Chaboki, A., 1984, "Jet-Impingement Heat Transfer for a Circular Jet Impinging in Crossflow on a Cylinder," ASME J. Heat Transfer, **106**(3), pp. 570-577.

[17] Tawfek, A. A., 1999, "Heat Transfer due to a Round Jet Impinging Normal to a Circular Cylinder," Heat Mass Transfer, **35**(4), pp. 327-333.

[18] Singh, D., Premachandran, B., and Kohli, S., 2013, "Experimental and

Numerical Investigation of Jet Impingement Cooling of a Circular cylinder," Int. J. Heat Mass Transfer, **60**, pp. 672-688.

[19] Singh, D., Premachandran, B., and Kohli, S., 2013, "Numerical Simulation of the Jet Impingement Cooling of a Circular Cylinder," Numer. Heat Tr. A-Appl., **64**(2), pp. 153-185.

[20] Wang, X. L., Yan, H. B., Lu, T. J., Song, S. J., and Kim, T., 2014, "Heat Transfer Characteristics of an Inclined Impinging Jet on a Curved Surface in Crossflow," ASME J. Heat Transfer, **136**(8), p. 081702.

[21] Wang, X. L., Lee, J. H., Lu, T. J., Song, S. J., and Kim, T., 2014, "A Comparative Study of Single-/Two-jet Crossflow Heat Transfer on a Circular Cylinder," Int. J. Heat Mass Transfer, **78**, pp. 588-598.

[22] Zukauskas, A., 1987, "Heat Transfer from Tubes in Crossflow," Adv. Heat Transfer, **18**, pp. 87-159.

[23] Hsueh, K. L., and Chin, D. T., 1986, "Mass Transfer of a Submerged Jet Impinging on a Cylindrical Surface," J. Electrochem. Soc., **133**(9), pp. 1845-1850.

[24] Bartoli, C., Di Marco, P., and Faggiani, S., 1993, "Impingement Heat Transfer at a Cylinder Due to a Submerged Slot Jet of Water," Exp. Therm. Fluid Sci., **7**(4), pp. 279-286.

[25] Fleischer, A. S., Kramer, K., and Goldstein, R. J., 2001, "Dynamics of the Vortex Structure of a Jet Impinging on a Convex Surface," Exp. Therm. Fluid Sci., **24**(4), pp. 169-175.

[26] Schuh, H., and Persson, B., 1964, "Heat Transfer on Circular Cylinders Exposed to Free-jet flow," Int. J. Heat Mass Transfer, **7**(11), pp. 1257-1271.

[27] Kumada, M., Mabuchi, I., and Kawashima, Y., 1973, "Mass Transfer on a

Cylinder in the Potential Core Region of a Two-Dimensional Jet," Heat Transfer – Japanese Research, **2**, pp. 53-66.

[28] Sparrow, E. M., and Alhomoud, A., 1984, "Impingement Heat Transfer at a Circular Cylinder Due to an Offset or Non-offset Slot Jet," Int. J. Heat Mass Transfer, **27**(12), pp. 2297-2306.

[29] Zdravkovich, M. M., 1997, "Flow around Cylinders Vol 1: Fundamentals," Oxford: Oxford Science Publications, p. 25.

[30] Bunker, R. S., Dees, J. E., and Palafox, P., 2014, "Impingement Cooling in Gas Turbines: Design, Applications, and Limitations," In: Amano, R.S. and Sunden, B., "Impingement Jet Cooling in Gas Turbines", Southampton: WIT Press, p.14-15.

[31] Yule, A. J., 1978, "Large-Scale Structure in the Mixing Layer of a Round Jet," J. Fluid Mech., **89**(3), pp. 413-432.

[32] Gautner, J. W., Livinggood, J. N. B., and Hrycak, P., 1970, "Survey of Literature on Flow Characteristics of a Single Turbulent Jet Impinging on a Flat Plate," NASA Technical Note D-5652.

[33] Abramovich, G. N., 1963, "The Theory of Turbulent Jets," Cambridge, Massachusetts: MIT Press.

[34] Desgeorges, O., Lee, T., and Kafyeke, F., 2002, "Multiple Hot-Film Sensor Array Calibration and Skin Friction Measurement," Exp. Fluids, **32**(1), pp. 37-43.

[35] Bellhouse, B., and Schultz, D. L., 1966, "Determination of Mean and Dynamic Skin Friction, Separation and Transition in Low-Speed Flow with a Thin-Film Heated Element," J. Fluid Mech., **24**(2), pp. 379-400.

[36] Wietrzak, A., and Lueptow, R. M., 1994, "Wall Shear Stress and Velocity

in a Turbulent Axisymmetric Boundary Layer," J. Fluid Mech., **259**, pp. 191-218.

[37] Holman, J. P., 1994, "Experimental Methods for Engineers," 6th ed., McGraw-Hill, pp. 49-56.

[38] Perry, A. E., 1982, "Hot-Wire Anemometry", Clarendon Press Oxford, pp. 132-138.

[39] Lighthill, M. J., 1945, "Note on the Deflection of Jets by Curved Surfaces, and on the Design of Bends in Wind Tunnels," Aeronautical Research Council Reports and Memoranda 2105.

[40] Wille, R., and Fernholz, H., 1965, "Report on the First European Mechanics Colloquium on the Coanda Effect," J. Fluid Mech., **23**(4), pp. 801-819.

[41] Aspelt, C. J., and West, G. S., 1975, "The Effects of Wake Splitter Plates on Bluff-body Flow in the Range $10^4 < R < 5 \times 10^4$. Part 2," J. Fluid Mech., **71**(1), pp. 145-160.

APPENDIX A

The static pressure distribution in the crossflow plane of a cylinder subject to the impingement of a round jet [14] and immersed in a uniform stream [41] is depicted in Fig. 16 for Re_D = 50,000. The static pressure distribution has been generalised with a static pressure coefficient (C_p):

$$C_p = \frac{p(\alpha) - p_{amb}}{\frac{1}{2}\rho w_e^{\,2}} \tag{6}$$

Here, p_{amb} represents ambient pressure, ρ represents the density of air, w_e represents the centreline velocity at the jet exit and $p(\alpha)$ represents the static pressure at the point where C_p is being defined.

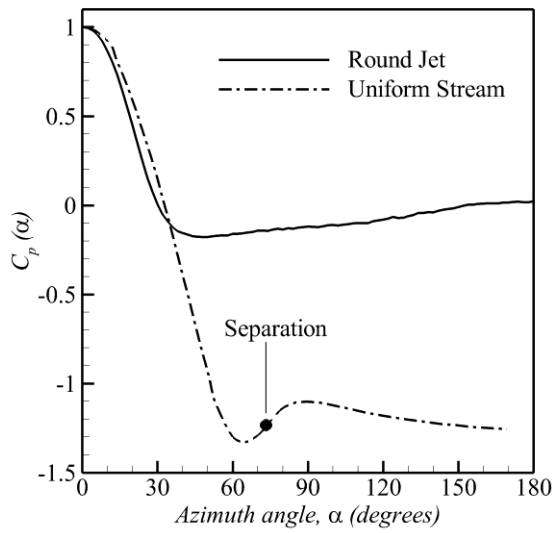

Figure 16. Static pressure distribution in the crossflow plane of a cylinder subject to the impingement of a round jet [14] and immersed in a uniform stream [41] at Re_D = 50,000

초 록

포텐셜 코어 안에서의 원기둥과 원형제트의 충돌

터빈 날개의 내부유동 냉각에 있어서 날개 뒷전의 원기둥 냉각은 자주 사용되는 냉각 방법이다. 날개 종류에 따라서 원기둥 냉각은 관통된 통로, 혹은 차폐, 유동 냉각을 이용하며 이러한 차폐는 유동의 난류를 증가시킨다. 하지만 이러한 냉각 방법에서 의도되지 않은 현상이 나타나곤 하는데 이것이 날개 뒷전 원기둥의 원형제트 충돌이다. 따라서 이번 연구에서는 원형제트의 원기둥 충돌을 조사하였으며 실린더 주변의 열전달 분포를 공기역학적으로 설명한다. 제트의 난류 혼합층과 원기둥 위에서 성장하는 층류 경계층의 결합으로 인한 경계층 천이가 원기둥 위 두번째 열전달률 최고점을 유발하는 것이 새로이 발견되었다. 이러한 결합은 포텐셜 코어유동을 종료시킴으로써 점성제트를 형성하여 벽으로부터 운동량을 분산시켜 열전달률의 점진적 감소와

경계층 박리를 촉진시킨다. 하지만 이러한 결합은 또한 난류와 곡률 유동이 열전달률이 일정한 값을 가지게 되는 원형 기둥 후류 유동의 경계층 박리를 지연 시킨다.

주요어: 터빈 날개 냉각; 차폐; 원형제트 충돌; 원형기둥

학 번: 2013-23824